arXiv:1410.0848v1 [physics.comp-ph] 3 Oct 2014

Determination of normalized magnetic eigenfields in microwave cavities

Johan Helsing* and Anders Karlsson†

October 6, 2014

Abstract

The magnetic field integral equation for axially symmetric cavities with perfectly conducting surfaces is discretized according to a high-order convergent Fourier–Nyström scheme. The resulting solver is used to determine eigenwavenumbers and normalized magnetic eigenfields to very high accuracy in the entire computational domain.

1 Introduction

This work is on the numerical solution of the time harmonic Maxwell equations in axially symmetric hollow microwave cavities with smooth and perfectly electric conducting (PEC) surfaces. We use the magnetic field integral equation (MFIE) and high-order convergent Fourier–Nyström discretization to find normalized magnetic eigenfields to high accuracy.

Particle accelerators are the most common application for microwave cavities, also known as Radio Frequency (RF) cavities. Today, all high energy particle accelerators use such cavities for particle acceleration by means of eigenfields, excited by external sources. The cavities consist of one, or several, axially symmetric cells, where in each cell the excited eigenfield corresponds to the TM_{010} mode in a cylindrical cavity, see [30, Chapter 1]. In addition to the eigenfields excited by the external sources, there are wakefields that consist of a large number of higher-order modes (HOM). The wakefields are excited in cavities and flanges by the beam of particles. See [30, Chapter 11] for a more detailed discussion. The wakefields affect the trajectories of the particles and, by that, the quality of the beam. To prevent that harmful wakefields are excited in the accelerator, numerical simulations are used both in its design process and during operation. These simulations need to cover a frequency band up to at least 10 times the frequency of the external source. At the highest frequency the width of each

*Centre for Mathematical Sciences, Lund University, Sweden
†Electrical and Information Technology, Lund University, Sweden

cell of a cavity is on the order of 5-10 wavelengths and the length on the order of 3-6 wavelengths. Accelerators can have cavities with as many as 20 cells. In the collaboration of the present authors with scientists at the synchrotron light source MAX IV and the European Spallation Source (ESS), both under construction in Lund, Sweden, we see a great need for improved numerical tools for accurate wakefield evaluation at higher frequencies. This is a motivation for our work.

During the last 30 years, software packages have become increasingly important for the design of microwave cavities. Today, finite element method (FEM) based software packages like COMSOL Multiphysics, ANSYS, and HFSS, finite difference method (FD and FDTD) based packages like SUPERFISH [16] and GdfidL [8], and finite integration technique (FIT) [33] based packages like MAFIA and CST, are common design tools. All of these packages rely on a partial differential equation (PDE) formulation of the time harmonic Maxwell equations and they discretize the volume, or, in the axially symmetric case, the cross section of the cavity. They are suitable for evaluations of low-order modes in cavities, but less suitable for accurate evaluations of high-frequency wakefields, due to their relatively low-order convergence.

To our knowledge, there are no published papers on the MFIE applied to microwave cavities. Neither have we found any published benchmark results. Authors using the MFIE in axially symmetric domains apply it to exterior problems and the same is true for the related electric field integral equation (EFIE) and the combined field integral equation (CFIE). The method of moments (MoM) is the most common method for discretization, see [2], [14], [22], and the reference list in [28]. Only a few papers favor Nyström methods, see [12] and [29]. The CFIE is often used for exterior problems since, in contrast to MFIE and EFIE, it provides unique solutions also at the eigenwavenumbers of the interior problem. For the interior problem, CFIE is unnecessarily complicated. An alternative to CFIE is presented in [10] and [11], where two coupled surface integral equations with unique solutions are derived by introducing surface potentials, referred to as Debye sources.

The present work shows that high-order convergent Nyström schemes for the MFIE can be efficiently implemented when applied to cavities with PEC surfaces. Very accurate results are obtained both for surface current densities and for surface charge densities at a broad range of eigenwavenumbers. These results can, via a post-processor, be carried over to normalized magnetic eigenfields at all positions inside the cavity, also close to surfaces where integral equation techniques usually encounter difficulties. Our post-processor takes advantage of a new surface integral expression for the normalization. In terms of discretization techniques used, we rely solely on [19]. In [19] we developed an explicit kernel-split panel-based Fourier–Nyström scheme for integral equations on axially symmetric surfaces where the integral operators can have weakly singular or Cauchy-type singular kernels.

The numerical examples in [19] deal with acoustic eigenfields and only require the discretization of three distinct integral operators. The numerical examples of the present work involve around 30 distinct, but very similar, integral operators. They are all discretized using techniques from [19]. See [34] for a related Nyström scheme, without kernel splits, in the acoustic setting.

The paper is organized as follows: Section 2 presents the MFIE and an integral representation of the magnetic field in a concise notation. Section 3 defines an azimuthal Fourier transformation of 2π-periodic functions and applies it to the MFIE and to the field representation. Section 4 reviews our Nyström discretization scheme for transformed integral operators and equations. Section 5 contains numerical examples with relevance to accelerator technology and nano-optics. The conclusions in Section 6 relate to future research directions. In order to maintain a high narrative pace in the main body of the paper we have collected some rather important details in three appendices. Appendix A contains a derivation of the surface integral expression used for the normalization. Appendix B presents a number of useful relations between various layer densities and potentials. Appendix C gives a short MATLAB code for the accurate evaluation of two half-integer Legendre functions.

2 Problem formulation

This section introduces the MFIE for the time harmonic Maxwell equations in a notation that is particularly adapted to axially symmetric hollow cavities with PEC surfaces. Most of the material is well known, see [12, 14, 15, 22].

2.1 Basic notation

Let Γ be an axially symmetric surface enclosing a three-dimensional domain V (a body of revolution) and let

$$\boldsymbol{r} = (x, y, z) = (\rho\cos\theta, \rho\sin\theta, z) \tag{1}$$

denote a point in $\mathbb{R}^3$. Here $\rho = \sqrt{x^2 + y^2}$ is the distance from the z-axis and θ is the azimuthal angle. The outward unit normal $\boldsymbol{\nu}$ at a point $\boldsymbol{r}$ on Γ is defined as

$$\boldsymbol{\nu} = (\nu_\rho\cos\theta, \nu_\rho\sin\theta, \nu_z)\,. \tag{2}$$

We also need the unit vectors

$$\boldsymbol{\rho} = (\cos\theta, \sin\theta, 0)\,, \tag{3}$$

$$\boldsymbol{\theta} = (-\sin\theta, \cos\theta, 0)\,, \tag{4}$$

$$\boldsymbol{\tau} = \boldsymbol{\theta}\times\boldsymbol{\nu} = (\nu_z\cos\theta, \nu_z\sin\theta, -\nu_\rho)\,, \tag{5}$$

$$\boldsymbol{z} = (0, 0, 1)\,, \tag{6}$$

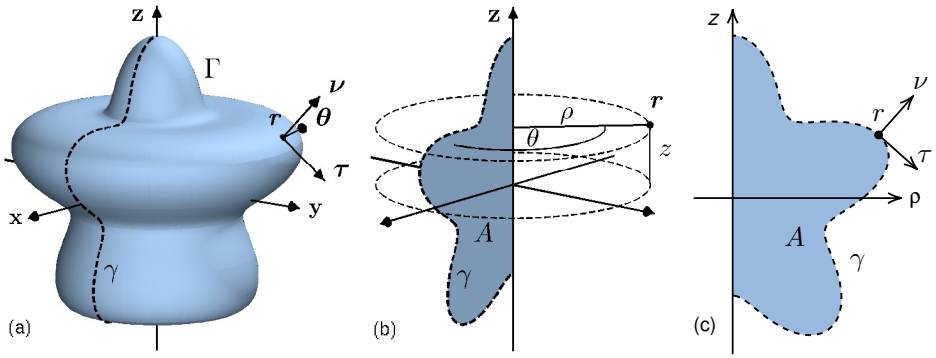

Figure 1: An axisymmetric surface Γ generated by a curve γ. (a) A point $\boldsymbol{r}$ on Γ has outward unit normal $\boldsymbol{\nu}$ and tangent vector $\boldsymbol{\tau}$. (b) $\boldsymbol{r}$ has radial distance ρ, azimuthal angle θ, and height z. The planar domain A is bounded by γ and the z-axis. (c) Coordinate axes and vectors in the half-plane $\mathbb{R}^{2+}$.

where $\boldsymbol{\theta}$ and $\boldsymbol{\tau}$ are two tangential unit vectors. See Figure 1(a) and 1(b).

The angle $\theta = 0$ defines a half-plane $\mathbb{R}^{2+}$ in $\mathbb{R}^3$ whose intersection with Γ corresponds to a generating curve γ. Let $r = (\rho, z)$ be a point in $\mathbb{R}^{2+}$ and let A be the planar domain bounded by γ and the z-axis. The outward unit normal on γ is $\nu = (\nu_\rho, \nu_z)$ and $\tau = (\nu_z, -\nu_\rho)$ is a tangent. See Figure 1(b) and 1(c). The unit vectors in the ρ- and z-directions are $\hat{\rho}$ and $\hat{z}$.

2.2 PDE formulation

Our primary interest is the magnetic field. With vacuum in V and with Γ perfectly conducting, the magnetic field $\boldsymbol{H}(\boldsymbol{r})$ satisfies the following system of partial differential equations

$$\nabla^2 \boldsymbol{H}(\boldsymbol{r}) + k^2 \boldsymbol{H}(\boldsymbol{r}) = \boldsymbol{0}\,, \qquad \boldsymbol{r} \in V\,, \tag{7}$$

$$\nabla \cdot \boldsymbol{H}(\boldsymbol{r}) = 0\,, \qquad \boldsymbol{r} \in V\,, \tag{8}$$

with boundary condition

$$\lim_{V \ni \boldsymbol{r} \to \boldsymbol{r}^\circ} \boldsymbol{\nu}^\circ \times (\nabla \times \boldsymbol{H}(\boldsymbol{r})) = \boldsymbol{0}\,, \qquad \boldsymbol{r}^\circ \in \Gamma\,. \tag{9}$$

We will find nontrivial solutions to these equations in a fast and accurate fashion via the MFIE.

The values k^2 for which the system (7), (8), and (9) admits nontrivial solutions are called eigenvalues. We refer to the corresponding fields $\boldsymbol{H}(\boldsymbol{r})$ as magnetic eigenfields and to k as eigenwavenumbers. The eigenvalues constitute a real, positive and countable set, accumulating only at infinity [32]. The eigenvalues have finite multiplicity. Magnetic eigenfields that correspond to distinct eigenvalues are orthogonal and subspaces of magnetic

eigenfields that correspond to particular eigenvalues can be given orthogonal bases.

We introduce an inner product on V, denoted by angle brackets $\langle \cdot, \cdot \rangle$, and an induced norm

$$\langle \boldsymbol{F}, \boldsymbol{G} \rangle = \int_V \boldsymbol{F}^*(\boldsymbol{r}) \cdot \boldsymbol{G}(\boldsymbol{r}) \, \mathrm{d}V \,, \qquad \|\boldsymbol{F}\|^2 = \langle \boldsymbol{F}, \boldsymbol{F} \rangle \,. \tag{10}$$

Here $\boldsymbol{F}(\boldsymbol{r})$ and $\boldsymbol{G}(\boldsymbol{r})$ are vector (or scalar) fields on V and the symbol '$*$' denotes the complex conjugate. Magnetic eigenfields $\boldsymbol{H}(\boldsymbol{r})$ are normalized so that

$$\|\boldsymbol{H}\|^2 \equiv \int_V \boldsymbol{H}^*(\boldsymbol{r}) \cdot \boldsymbol{H}(\boldsymbol{r}) \, \mathrm{d}V = 1 \,. \tag{11}$$

The volume integral in (11) is referred to as *the normalization integral*. In Appendix A it is reformulated as a surface integral that is well suited for numerical evaluation in the framework of the MFIE.

2.3 The MFIE

The magnetic field is represented in terms of the surface current density

$$\boldsymbol{J}_{\mathrm{s}}(\boldsymbol{r}^\circ) = \lim_{V \ni \boldsymbol{r} \to \boldsymbol{r}^\circ} -\boldsymbol{\nu}^\circ \times \boldsymbol{H}(\boldsymbol{r}) \,, \qquad \boldsymbol{r}^\circ \in \Gamma \,, \tag{12}$$

by the Stratton–Chu integral representation [26, 31]. When (9) holds, this representation assumes the form

$$\left.\begin{matrix} \boldsymbol{H}(\boldsymbol{r}) \\ \boldsymbol{0} \end{matrix}\right\} = \nabla \times \int_\Gamma \boldsymbol{J}_{\mathrm{s}}(\boldsymbol{r}') \Phi_k(\boldsymbol{r}, \boldsymbol{r}') \, \mathrm{d}\Gamma' \quad \begin{cases} \boldsymbol{r} \in V \,, \\ \boldsymbol{r} \in \mathbb{R}^3 \setminus V \cup \Gamma \,, \end{cases} \tag{13}$$

where, using the time dependence $e^{-\mathrm{i}\omega t}$,

$$\Phi_k(\boldsymbol{r}, \boldsymbol{r}') = \frac{e^{\mathrm{i}k|\boldsymbol{r}-\boldsymbol{r}'|}}{4\pi|\boldsymbol{r}-\boldsymbol{r}'|} \tag{14}$$

is the causal fundamental solution to the Helmholtz equation. The upper equation in (13) gives the magnetic field in V. The lower equation states that $\boldsymbol{J}_{\mathrm{s}}(\boldsymbol{r})$ induces a zero magnetic field outside Γ.

Taking the limit $V \ni \boldsymbol{r} \to \boldsymbol{r}^\circ \in \Gamma$ in (13) and using (12), one gets the MFIE:

$$\frac{1}{2}\boldsymbol{J}_{\mathrm{s}}(\boldsymbol{r}) - \boldsymbol{\nu} \times \int_\Gamma \big(\boldsymbol{J}_{\mathrm{s}}(\boldsymbol{r}') \times \nabla \Phi_k(\boldsymbol{r}, \boldsymbol{r}') \big) \, \mathrm{d}\Gamma' = \boldsymbol{0} \,, \qquad \boldsymbol{r} \in \Gamma \,. \tag{15}$$

A solution to the MFIE, together with (13), is also a solution to the system (7), (8), and (9). The kernel of the integral operator in the MFIE is weakly singular, whereas the kernel in (13) exhibits a stronger singularity in the limit $\mathbb{R}^3 \setminus \Gamma \ni \boldsymbol{r} \to \boldsymbol{r}^\circ \in \Gamma$.

In order to cast (15) in a form more suitable for numerical solution we decompose $\boldsymbol{J}_{\rm s}(\boldsymbol{r})$ in its tangential components

$$\boldsymbol{J}_{\rm s}(\boldsymbol{r}) = \boldsymbol{\tau} J_\tau(\boldsymbol{r}) + \boldsymbol{\theta} J_\theta(\boldsymbol{r}) \tag{16}$$

and rewrite and split (15) into the two coupled scalar equations

$$\begin{aligned}
&J_\tau(\boldsymbol{r}) - 2\int_\Gamma \big((\boldsymbol{\tau}\cdot\boldsymbol{\tau}')J_\tau(\boldsymbol{r}') + (\boldsymbol{\tau}\cdot\boldsymbol{\theta}')J_\theta(\boldsymbol{r}')\big)\,\big(\boldsymbol{\nu}\cdot\nabla\Phi_k(\boldsymbol{r},\boldsymbol{r}')\big)\,\mathrm{d}\Gamma' \\
&\qquad + 2\int_\Gamma \big((\boldsymbol{\nu}\cdot\boldsymbol{\tau}')J_\tau(\boldsymbol{r}') + (\boldsymbol{\nu}\cdot\boldsymbol{\theta}')J_\theta(\boldsymbol{r}')\big)\,\big(\boldsymbol{\tau}\cdot\nabla\Phi_k(\boldsymbol{r},\boldsymbol{r}')\big)\,\mathrm{d}\Gamma' = 0\,, \\
&J_\theta(\boldsymbol{r}) - 2\int_\Gamma \big((\boldsymbol{\theta}\cdot\boldsymbol{\tau}')J_\tau(\boldsymbol{r}') + (\boldsymbol{\theta}\cdot\boldsymbol{\theta}')J_\theta(\boldsymbol{r}')\big)\,\big(\boldsymbol{\nu}\cdot\nabla\Phi_k(\boldsymbol{r},\boldsymbol{r}')\big)\,\mathrm{d}\Gamma' \\
&\qquad + 2\int_\Gamma \big((\boldsymbol{\nu}\cdot\boldsymbol{\tau}')J_\tau(\boldsymbol{r}') + (\boldsymbol{\nu}\cdot\boldsymbol{\theta}')J_\theta(\boldsymbol{r}')\big)\,\big(\boldsymbol{\theta}\cdot\nabla\Phi_k(\boldsymbol{r},\boldsymbol{r}')\big)\,\mathrm{d}\Gamma' = 0\,.
\end{aligned} \tag{17}$$

It is convenient to express the system (17) in the more compact form

$$\begin{aligned}
(I+K_1)\,J_\tau(\boldsymbol{r}) + \mathrm{i}K_2 J_\theta(\boldsymbol{r}) &= 0\,, \qquad \boldsymbol{r}\in\Gamma\,, \\
\mathrm{i}K_3 J_\tau(\boldsymbol{r}) + (I+K_4)\,J_\theta(\boldsymbol{r}) &= 0\,, \qquad \boldsymbol{r}\in\Gamma\,.
\end{aligned} \tag{18}$$

Here I is the identity. The double-layer type operators K_α, with kernels $K_\alpha(\boldsymbol{r},\boldsymbol{r}')$, are defined by their actions on a layer density $g(\boldsymbol{r})$ on Γ as

$$K_\alpha g(\boldsymbol{r}) = \int_\Gamma K_\alpha(\boldsymbol{r},\boldsymbol{r}')g(\boldsymbol{r}')\,\mathrm{d}\Gamma' = \int_\Gamma D_\alpha(\boldsymbol{r},\boldsymbol{r}')P(\boldsymbol{r},\boldsymbol{r}')g(\boldsymbol{r}')\,\mathrm{d}\Gamma'\,, \tag{19}$$

where $\alpha = 1,2,3,4$,

$$D_1(\boldsymbol{r},\boldsymbol{r}') = 2\frac{\big(\rho\nu'_\rho - (\nu'\cdot r' - \nu'_z z)\cos(\theta-\theta')\big)}{4\pi|\boldsymbol{r}-\boldsymbol{r}'|^3}\,, \tag{20}$$

$$D_2(\boldsymbol{r},\boldsymbol{r}') = -2\mathrm{i}\frac{(z-z')\sin(\theta-\theta')}{4\pi|\boldsymbol{r}-\boldsymbol{r}'|^3}\,, \tag{21}$$

$$D_3(\boldsymbol{r},\boldsymbol{r}') = 2\mathrm{i}\frac{(\nu'_z\nu\cdot r - \nu_z\nu'\cdot r')\sin(\theta-\theta')}{4\pi|\boldsymbol{r}-\boldsymbol{r}'|^3}\,, \tag{22}$$

$$D_4(\boldsymbol{r},\boldsymbol{r}') = -2\frac{(\rho'\nu_\rho - (\nu\cdot r - \nu_z z')\cos(\theta-\theta'))}{4\pi|\boldsymbol{r}-\boldsymbol{r}'|^3}\,, \tag{23}$$

and

$$P(\boldsymbol{r},\boldsymbol{r}') = (1-\mathrm{i}k|\boldsymbol{r}-\boldsymbol{r}'|)e^{\mathrm{i}k|\boldsymbol{r}-\boldsymbol{r}'|}\,, \tag{24}$$

$$|\boldsymbol{r}-\boldsymbol{r}'| = \sqrt{\rho^2+\rho'^2-2\rho\rho'\cos(\theta-\theta')+(z-z')^2}\,. \tag{25}$$

The functions $D_\alpha(\boldsymbol{r},\boldsymbol{r}')$ can be viewed as static kernels, corresponding to wavenumber $k=0$.

2.4 Expressions for the magnetic field

The magnetic field (13) can be expressed in a form analogous to (18), which is better suited for numerics. For this, we introduce the decomposition

$$\boldsymbol{H}(\boldsymbol{r}) = \boldsymbol{\rho} H_\rho(\boldsymbol{r}) + \boldsymbol{\theta} H_\theta(\boldsymbol{r}) + \boldsymbol{z} H_z(\boldsymbol{r})\,. \tag{26}$$

Straightforward calculations give for $\boldsymbol{r} \in \mathbb{R}^3 \setminus \Gamma$

$$\begin{aligned} H_\rho(\boldsymbol{r}) &= \mathrm{i}K_5 J_\tau(\boldsymbol{r}) + K_6 J_\theta(\boldsymbol{r})\,, \\ H_\theta(\boldsymbol{r}) &= K_7 J_\tau(\boldsymbol{r}) + \mathrm{i}K_8 J_\theta(\boldsymbol{r})\,, \\ H_z(\boldsymbol{r}) &= \mathrm{i}K_9 J_\tau(\boldsymbol{r}) + K_{10} J_\theta(\boldsymbol{r})\,, \end{aligned} \tag{27}$$

where K_α, $\alpha = 5, 6, 7, 8, 9, 10$, are defined as in (19) with

$$D_5(\boldsymbol{r}, \boldsymbol{r}') = -\mathrm{i}\frac{(\nu' \cdot r' - \nu_z' z)\sin(\theta - \theta')}{4\pi|\boldsymbol{r} - \boldsymbol{r}'|^3}\,, \tag{28}$$

$$D_6(\boldsymbol{r}, \boldsymbol{r}') = \frac{(z - z')\cos(\theta - \theta')}{4\pi|\boldsymbol{r} - \boldsymbol{r}'|^3}\,, \tag{29}$$

$$D_7(\boldsymbol{r}, \boldsymbol{r}') = -\frac{\big(\nu_\rho' \rho - (\nu' \cdot r' - \nu_z' z)\cos(\theta - \theta')\big)}{4\pi|\boldsymbol{r} - \boldsymbol{r}'|^3}\,, \tag{30}$$

$$D_8(\boldsymbol{r}, \boldsymbol{r}') = \mathrm{i}\frac{(z - z')\sin(\theta - \theta')}{4\pi|\boldsymbol{r} - \boldsymbol{r}'|^3}\,, \tag{31}$$

$$D_9(\boldsymbol{r}, \boldsymbol{r}') = -\mathrm{i}\frac{\nu_z' \rho \sin(\theta - \theta')}{4\pi|\boldsymbol{r} - \boldsymbol{r}'|^3}\,, \tag{32}$$

$$D_{10}(\boldsymbol{r}, \boldsymbol{r}') = \frac{\rho' - \rho\cos(\theta - \theta')}{4\pi|\boldsymbol{r} - \boldsymbol{r}'|^3}\,. \tag{33}$$

3 Fourier series expansions

The aim of this paper is to present a high-order convergent and accurate discretization scheme to solve the MFIE and to to evaluate magnetic eigenfields, normalized by (11). We employ a Fourier–Nyström technique where the first step is an azimuthal Fourier transformation of the MFIE system (18) and of the system for the decomposed magnetic field (27).

Several 2π-periodic quantities need to be expanded. We define the azimuthal Fourier coefficients

$$g_n(r) = \frac{1}{\sqrt{2\pi}} \int_{-\pi}^{\pi} e^{-\mathrm{i}n\theta} g(\boldsymbol{r})\,\mathrm{d}\theta\,, \tag{34}$$

$$G_n(r, r') = \frac{1}{\sqrt{2\pi}} \int_{-\pi}^{\pi} e^{-\mathrm{i}n(\theta - \theta')} G(\boldsymbol{r}, \boldsymbol{r}')\,\mathrm{d}(\theta - \theta')\,, \tag{35}$$

where $g(\boldsymbol{r})$ can represent functions like $J_\tau(\boldsymbol{r})$, $J_\theta(\boldsymbol{r})$, $H_\rho(\boldsymbol{r})$, $H_\theta(\boldsymbol{r})$, and $H_z(\boldsymbol{r})$ and where $G(\boldsymbol{r}, \boldsymbol{r}')$ can represent functions like $K_\alpha(\boldsymbol{r}, \boldsymbol{r}')$, $D_\alpha(\boldsymbol{r}, \boldsymbol{r}')$,

and $P(\boldsymbol{r}, \boldsymbol{r}')$. The subscript n is the azimuthal index. The coefficients $G_n(r, r')$ may also be called transformed kernels or modal Green's functions.

Expansion and integration of (18) and (27) over θ' give the system of modal integral equations

$$\begin{aligned} \left(I + \sqrt{2\pi}K_{1n}\right) J_{\tau n}(r) + \mathrm{i}\sqrt{2\pi}K_{2n}J_{\theta n}(r) = 0\,, \qquad r \in \gamma\,, \\ \mathrm{i}\sqrt{2\pi}K_{3n}J_{\tau n}(r) + \left(I + \sqrt{2\pi}K_{4n}\right) J_{\theta n}(r) = 0\,, \qquad r \in \gamma\,, \end{aligned} \tag{36}$$

and the modal representation of the magnetic field for $r \in \mathbb{R}^{2+} \setminus \gamma$

$$\begin{aligned} H_{\rho n}(r) &= \mathrm{i}\sqrt{2\pi}K_{5n}J_{\tau n}(r) + \sqrt{2\pi}K_{6n}J_{\theta n}(r)\,, \\ H_{\theta n}(r) &= \sqrt{2\pi}K_{7n}J_{\tau n}(r) + \mathrm{i}\sqrt{2\pi}K_{8n}J_{\theta n}(r)\,, \\ H_{zn}(r) &= \mathrm{i}\sqrt{2\pi}K_{9n}J_{\tau n}(r) + \sqrt{2\pi}K_{10n}J_{\theta n}(r)\,. \end{aligned} \tag{37}$$

The azimuthal index is $n = 0, \pm 1, \pm 2, \ldots$ and

$$K_{\alpha n}g_n(r) = \int_\gamma K_{\alpha n}(r, r')g_n(r')\rho'\,\mathrm{d}\gamma'\,, \qquad \alpha = 1, \ldots, 10\,. \tag{38}$$

3.1 Azimuthal Fourier coefficients in closed form

When r and r' are far apart, the kernels $K_\alpha(\boldsymbol{r}, \boldsymbol{r}')$ are smooth functions and the $K_{\alpha n}(r, r')$, present in (36) and (37), can be efficiently evaluated from (35) using discrete Fourier transform techniques (FFT). When $r \approx r'$, this is not true. Then it is more economical to split each $K_\alpha(\boldsymbol{r}, \boldsymbol{r}')$ into two terms: a smooth term, which is transformed via FFT, and a non-smooth term, which is transformed by convolution of $D_{\alpha n}(r, r')$ with parts of $P_n(r, r')$. See [19, Section 6] for details. We use $2N + 1 - n$ terms in the convolutions, where N is an integer controlling all FFT operations.

The coefficients $D_{\alpha n}(r, r')$, for $r \approx r'$, are also costly to evaluate from (35). Fortunately, the $D_{\alpha n}(r, r')$ can be obtained as closed-form expressions involving half-integer degree Legendre functions of the second kind

$$\mathfrak{Q}_{n-\frac{1}{2}}(\chi) = \int_{-\pi}^{\pi} \frac{\cos(nt)\,\mathrm{d}t}{\sqrt{8\,(\chi - \cos(t))}}\,, \tag{39}$$

which are cheap to evaluate. The functions $\mathfrak{Q}_{n-\frac{1}{2}}(\chi)$, with real arguments $\chi \geq 1$, may also be called toroidal harmonics [24]. They are symmetric with

respect to n and exhibit logarithmic singularities at $\chi = 1$. Introducing

$$\eta = \left(8\pi^3 \rho\rho'\right)^{-\frac{1}{2}} , \tag{40}$$

$$\chi = 1 + \frac{|r - r'|^2}{2\rho\rho'} , \tag{41}$$

$$d(\nu) = \frac{\nu \cdot (r - r')}{|r - r'|^2} , \tag{42}$$

$$\mathfrak{R}_n(\chi) = \frac{2n-1}{\chi+1} \left(\chi \mathfrak{Q}_{n-\frac{1}{2}}(\chi) - \mathfrak{Q}_{n-\frac{3}{2}}(\chi) \right) , \tag{43}$$

one can write

$$D_{1n}(r, r') = -2\eta \left[d(\nu') \mathfrak{R}_n(\chi) - \frac{(\nu' \cdot r' - \nu'_z z)}{2\rho\rho'} \left(\mathfrak{R}_n(\chi) + \mathfrak{Q}_{n-\frac{1}{2}}(\chi) \right) \right] , \tag{44}$$

$$D_{2n}(r, r') = -2\eta \frac{(z - z')}{\rho\rho'} n \mathfrak{Q}_{n-\frac{1}{2}}(\chi) , \tag{45}$$

$$D_{3n}(r, r') = 2\eta \frac{(\nu'_z \nu \cdot r - \nu_z \nu' \cdot r')}{\rho\rho'} n \mathfrak{Q}_{n-\frac{1}{2}}(\chi) , \tag{46}$$

$$D_{4n}(r, r') = -2\eta \left[d(\nu) \mathfrak{R}_n(\chi) + \frac{(\nu \cdot r - \nu_z z')}{2\rho\rho'} \left(\mathfrak{R}_n(\chi) + \mathfrak{Q}_{n-\frac{1}{2}}(\chi) \right) \right] , \tag{47}$$

and

$$D_{5n}(r, r') = -\eta \frac{(\nu' \cdot r' - \nu'_z z)}{\rho\rho'} n \mathfrak{Q}_{n-\frac{1}{2}}(\chi) , \tag{48}$$

$$D_{6n}(r, r') = -\eta \left[d(\hat{z}) \mathfrak{R}_n(\chi) + \frac{(z - z')}{2\rho\rho'} \left(\mathfrak{R}_n(\chi) + \mathfrak{Q}_{n-\frac{1}{2}}(\chi) \right) \right] , \tag{49}$$

$$D_{7n}(r, r') = \eta \left[d(\nu') \mathfrak{R}_n(\chi) - \frac{(\nu' \cdot r' - \nu'_z z)}{2\rho\rho'} \left(\mathfrak{R}_n(\chi) + \mathfrak{Q}_{n-\frac{1}{2}}(\chi) \right) \right] , \tag{50}$$

$$D_{8n}(r, r') = \eta \frac{(z - z')}{\rho\rho'} n \mathfrak{Q}_{n-\frac{1}{2}}(\chi) , \tag{51}$$

$$D_{9n}(r, r') = -\eta \frac{\nu'_z}{\rho'} n \mathfrak{Q}_{n-\frac{1}{2}}(\chi) , \tag{52}$$

$$D_{10n}(r, r') = \eta \left[d(\hat{\rho}) \mathfrak{R}_n(\chi) + \frac{1}{2\rho'} \left(\mathfrak{R}_n(\chi) + \mathfrak{Q}_{n-\frac{1}{2}}(\chi) \right) \right] . \tag{53}$$

Our derivation of (44–53) follows the procedure of Young, Hao, and Martinsson [34, Section 5.3]. The underlying idea – to expand the Green's function for the Laplacian in toroidal harmonics – is due to Cohl and Tohline [9]. The toroidal harmonics can be evaluated via a recursion whose forward form is

$$\mathfrak{Q}_{n-\frac{1}{2}}(\chi) = \frac{4n-4}{2n-1} \chi \mathfrak{Q}_{n-\frac{3}{2}}(\chi) - \frac{2n-3}{2n-1} \mathfrak{Q}_{n-\frac{5}{2}}(\chi) , \qquad n = 2, \ldots, N . \tag{54}$$

Appendix C contains the MATLAB function `toroharm` which evaluates the functions $\mathfrak{Q}_{-\frac{1}{2}}(\chi)$ and $\mathfrak{Q}_{\frac{1}{2}}(\chi)$, needed to initiate (54). The functions $\mathfrak{R}_n(\chi)$ of (43) are finite at $\chi = 1$, but have logarithmic singularities in their first (right) derivatives.

4 Nyström Discretization and kernel evaluation

Our Nyström discretization scheme along γ for the modal equations (36) and (37) and for the normalization integral of Appendix A is, essentially, identical to the scheme developed in [19] in a pure Helmholtz setting. This section only gives a brief review. The scheme relies on an underlying panel-based 16-point Gauss–Legendre quadrature with a mesh of n_{pan} quadrature panels on γ. The $16n_{\text{pan}}$ discretization points play the role of both target points r_i and source points r_j. The underlying quadrature is used in a conventional way when kernels $K_\alpha(\boldsymbol{r}, \boldsymbol{r}')$ are sufficiently smooth for $K_{\alpha n}(r_i, r_j)$ to be evaluated by FFT. For $r_i \approx r_j$, and when convolution is used for $K_{\alpha n}(r_i, r_j)$, an explicit kernel-split special quadrature is activated. Analytical information about the (near) singularities in $K_{\alpha n}(r, r')$ is exploited in the construction of 16th order accurate weight corrections, computed on the fly. As to some extent compensate for the loss of convergence order that comes with the special quadrature, a procedure of temporary mesh refinment is adopted. See [19], and also [17], for more information on these constructions and procedures.

4.1 The MFIE system and the decomposed magnetic field

It is worth emphasizing that all $K_{\alpha n}(r, r')$ are singular at $r = r'$ and that the singularities are inherited by the corresponding $D_{\alpha n}(r, r')$ of (44–53). The coefficients $D_{\alpha n}(r, r')$, $\alpha = 1, 2, 3, 4$, exhibit logarithmic singularities as $\gamma \ni r' \to r \in \gamma$. The coefficients $D_{\alpha n}(r, r')$, $\alpha = 5, 8, 9$, exhibit logarithmic singularities as $\mathbb{R}^{2+}\backslash\gamma \ni r \to r' \in \gamma$. The coefficients $D_{\alpha n}(r, r')$, $\alpha = 6, 7, 10$, generally exhibit logarithmic and Cauchy-type singularities as $\mathbb{R}^{2+}\backslash\gamma \ni r \to r' \in \gamma$. The quadratures constructed in [17, 19] cover all these situations.

The appearance of the closed-form expressions for $D_{\alpha n}(r, r')$ may seem somewhat intimidating at first glance. Nevertheless, the expressions are favorable from a computational perspective. The same toroidal functions repeat themselves, or occur in combination with smooth and simple functions independent of n. Remember that the $D_{\alpha n}(r_i, r_j)$ are convolved with parts of $P_n(r_i, r_j)$ to obtain $K_{\alpha n}(r_i, r_j)$ for $r_i \approx r_j$. Once $\mathfrak{Q}_{n-\frac{1}{2}}(\chi_{ij})$, $\mathfrak{R}_n(\chi_{ij})$, and $P_n(r_i, r_j)$, $n = 0, \ldots, N$, are evaluated and the convolution of $\mathfrak{Q}_{n-\frac{1}{2}}(\chi_{ij})$, $n\mathfrak{Q}_{n-\frac{1}{2}}(\chi_{ij})$, and $\mathfrak{R}_n(\chi_{ij})$ with parts of $P_n(r_i, r_j)$ is performed at all necessary combinations of r_i and r_j, the evaluation of $K_{\alpha n}(r_i, r_j)$, $\alpha = 1, 2, 3, 4$,

$r_i \approx r_j$, is very cheap. The evaluation of $K_{\alpha n}(r_i, r_j)$, $\alpha = 5, \ldots, 10$ requires a few more function evaluations and convolutions.

4.2 The normalization integral

Appendix A uses the scaled electric scalar potential $\Psi(\boldsymbol{r})$, the magnetic vector potential $\boldsymbol{\Lambda}(\boldsymbol{r})$, and the surface charge density $\varrho_{\mathrm{s}}(\boldsymbol{r})$. These quantities are related to $\boldsymbol{J}_{\mathrm{s}}(\boldsymbol{r})$ via

$$\Psi(\boldsymbol{r}) = S_\varsigma \varrho_{\mathrm{s}}(\boldsymbol{r})\,, \qquad \boldsymbol{r} \in \mathbb{R}^3\,, \tag{55}$$

$$\boldsymbol{\Lambda}(\boldsymbol{r}) = S_\varsigma \boldsymbol{J}_{\mathrm{s}}(\boldsymbol{r})\,, \qquad \boldsymbol{r} \in \mathbb{R}^3\,, \tag{56}$$

$$\varrho_{\mathrm{s}}(\boldsymbol{r}) = -\frac{\mathrm{i}}{k}\nabla_{\mathrm{s}} \cdot \boldsymbol{J}_{\mathrm{s}}(\boldsymbol{r}), \qquad \boldsymbol{r} \in \Gamma\,, \tag{57}$$

where $\nabla_{\mathrm{s}} \cdot (\ )$ is the surface divergence and S_ς is a single-layer type operator of the form

$$S_\alpha g(\boldsymbol{r}) = \int_\Gamma S_\alpha(\boldsymbol{r}, \boldsymbol{r}') g(\boldsymbol{r}')\,\mathrm{d}\Gamma' = \int_\Gamma Z_\alpha(\boldsymbol{r}, \boldsymbol{r}') e^{\mathrm{i}k|\boldsymbol{r}-\boldsymbol{r}'|} g(\boldsymbol{r}')\,\mathrm{d}\Gamma'\,, \tag{58}$$

with static kernel

$$Z_\varsigma(\boldsymbol{r}, \boldsymbol{r}') = \Phi_0(\boldsymbol{r}, \boldsymbol{r}') \quad \text{and} \quad Z_{\varsigma n}(r, r') = \eta \mathfrak{Q}_{n-\frac{1}{2}}(\chi)\,. \tag{59}$$

Azimuthal Fourier coefficients of $\Psi(\boldsymbol{r})$, $\boldsymbol{\Lambda}(\boldsymbol{r})$, and their normal- and tangetial derivatives need to be evaluated at discretization points r_j along γ. This, in turn, requires the introduction and discretization of several new and similar integral operators of the double-layer type (19) and of the single-layer type (58). It would, perhaps, carry too far to explicitly write up closed-form expressions for all $D_\alpha(\boldsymbol{r}, \boldsymbol{r}')$, $Z_\alpha(\boldsymbol{r}, \boldsymbol{r}')$, $D_{\alpha n}(r, r')$, and $Z_{\alpha n}(r, r')$ involved. The closed-form Fourier coefficients are derived using the same techniques as in Section 3.1. It is important to note that we avoid using (57) as a computational formula. Numerical differentiation leads to loss of precision and also to loss of convergence order in a panel-based setting. Rather, the surface charge density is obtained from the solution to a Fredholm second kind integral equation, as recommended in [29]. We also take advantage of two useful relations between $\boldsymbol{\Lambda}(\boldsymbol{r})$ and derivatives of $\Psi(\boldsymbol{r})$. Appendix B provides some detail.

5 Numerical examples

Our Fourier–Nyström scheme is implemented in MATLAB. The code was first verified by comparison with analytic solutions for the special case of Γ being the unit sphere [25, Chapter 9]. Eigenwavenumbers k corresponding to a few wavelengths across V gave coefficients $J_{\tau n}(r), J_{\theta n}(r)$, $r \in \gamma$, with relative L^2-errors of about 10^{-14} and coefficients $H_{\rho n}(r), H_{\theta n}(r), H_{zn}(r)$, $r \in A$, with

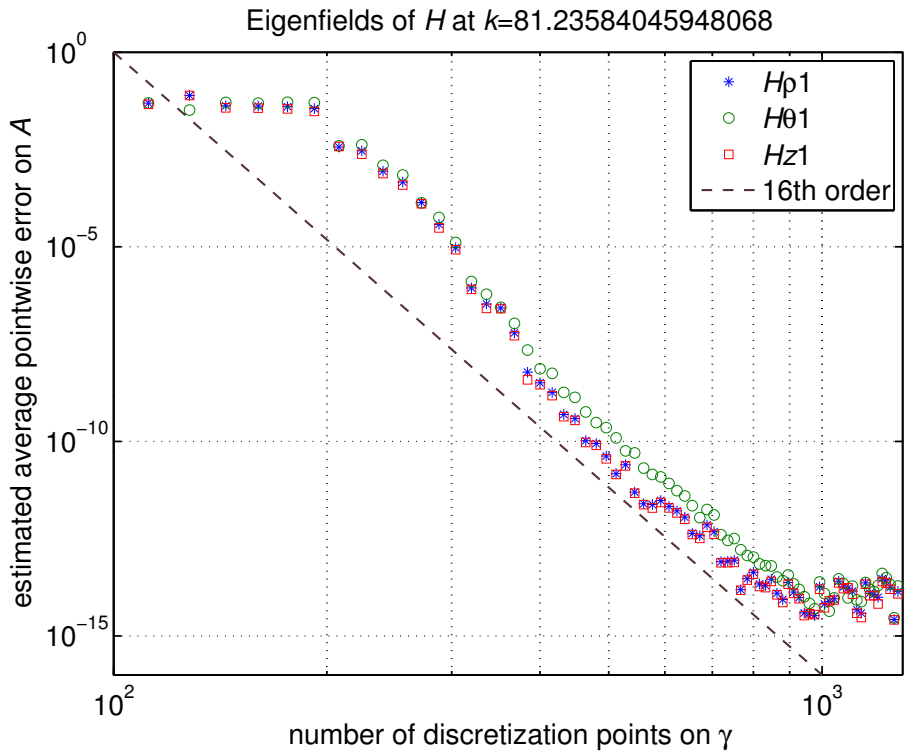

Figure 2: Convergence of the coefficients $H_{\rho 1}(r)$, $H_{\theta 1}(r)$, and $H_{z1}(r)$. The average accuracy has converged to between 13 and 14 digits at 864 discretization points on γ, corresponding to about 16 points per wavelength along γ.

pointwise errors of, typically, the same magnitude. Eigenwavenumbers corresponding to 32 wavelengths across V gave $J_{\tau n}(r), J_{\theta n}(r)$ with L^2-errors of about 10^{-13} and $H_{\rho n}(r), H_{\theta n}(r), H_{zn}(r)$ with pointwise errors ranging from 10^{-16} to 10^{-11}. The largest errors occurred for r close to γ in connection with high azimuthal indices n. We also compared evaluations of coefficients for the cavity with the star-shaped cross-section shown in Figure 1(a) with results obtained from COMSOL Multiphysics. Eigenwavenumbers corresponding to about two wavelengths across V gave results which agreed to all significant digits that COMSOL Multiphysics could produce.

We now present two more detailed numerical examples for the normalized magnetic eigenfields of the body of revolution in Figure 1(a). The purpose is to confirm that our solver meets many of the requirements imposed on a wakefield solver. The generating curve γ is parameterized as

$$r(t) = (\rho(t), z(t)) = (1 + 0.25\cos(5t))(\sin(t), \cos(t))\,, \qquad 0 \le t \le \pi\,, \quad (60)$$

which is the same curve that was used in the examples of [19]. The integer N, controlling FFT operations, is chosen as $N = \max\{120, 4n_{\text{pan}} + n\}$. The

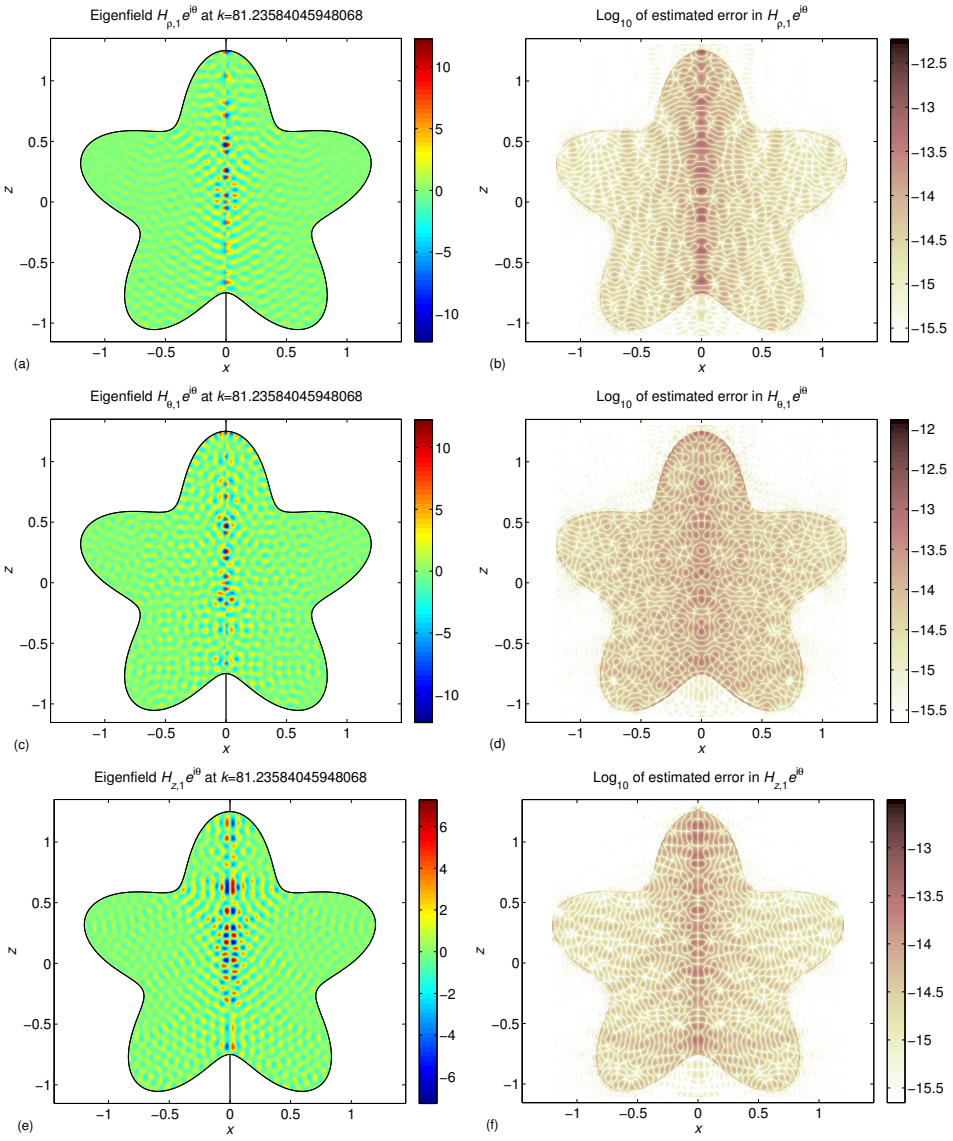

Figure 3: Left: (a), (c), (e) show $H_{\rho 1}(r)e^{\mathrm{i}\theta}$, $H_{\theta 1}(r)e^{\mathrm{i}\theta}$ and $H_{z1}(r)e^{\mathrm{i}\theta}$ at $k = 81.23584045948068$ and for $\theta = 0$ and $\theta = \pi$. Right: (b), (d), (f) show $\log_{10}$ of the estimated pointwise error with 1136 discretization points on γ.

MATLAB code is executed on a workstation equipped with an Intel Core i7 CPU at 3.20 GHz and 64 GB of memory.

The first example concerns an eigenfield with $k = 81.23584045948068$, corresponding to a generalized diameter of V of about 31 wavelengths, and $n = 1$. The MFIE is solved repeatedly on an increasingly refined uniform mesh. The coefficient vector $(H_{\rho 1}(r), H_{\theta 1}(r), H_{z1}(r))$ is evaluated at 25138 field points r, placed on a Cartesian grid in A. Figure 2 shows that our solver

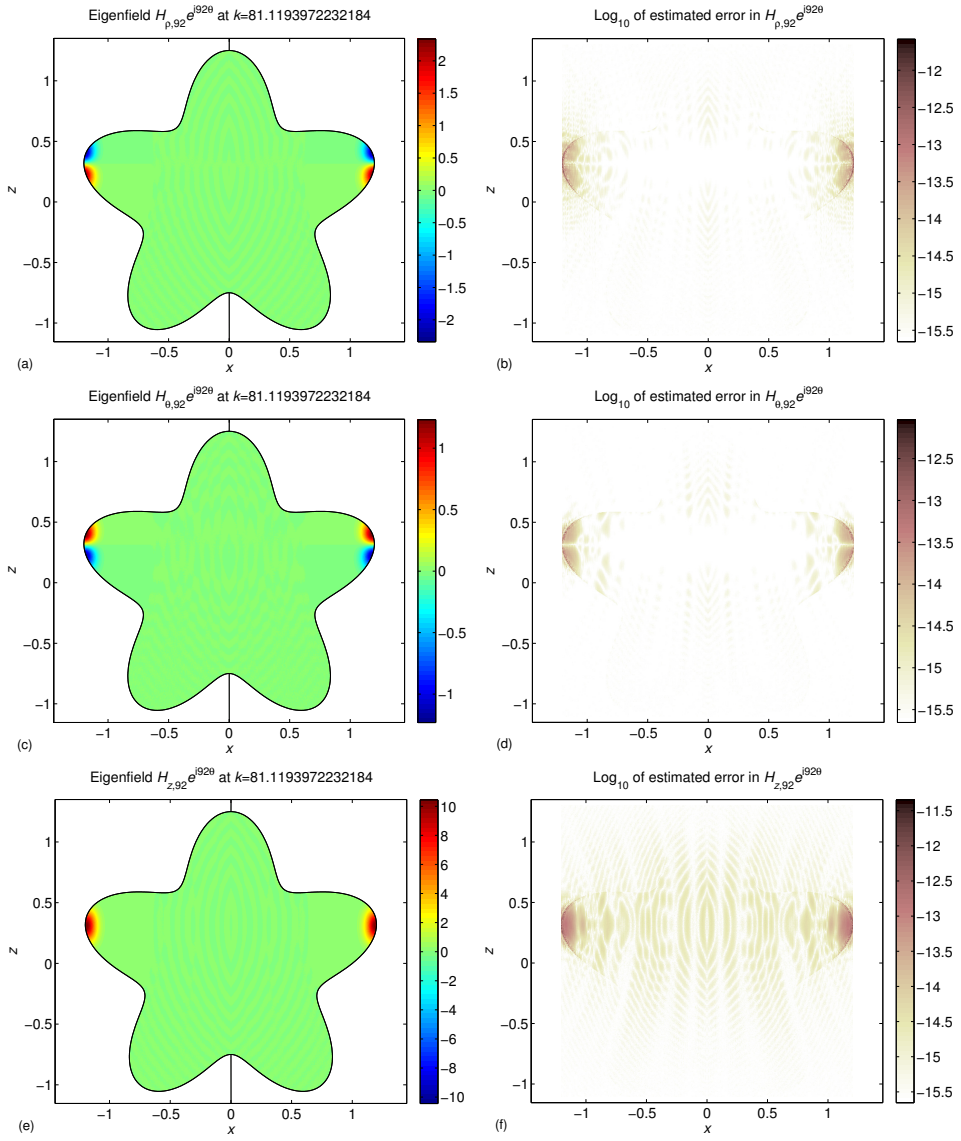

Figure 4: Left: (a), (c), (e) show $H_{\rho 92}(r)e^{\mathrm{i}92\theta}$, $H_{\theta 92}(r)e^{\mathrm{i}92\theta}$ and $H_{z92}(r)e^{\mathrm{i}92\theta}$ at $k = 81.1193972232184$ and for $\theta = 0$ and $\theta = \pi$. Right: (b), (d), (f) show $\log_{10}$ of the estimated pointwise error with 1024 discretization points on γ.

exhibits 16th order convergence, as expected. The *pointwise error* refers to an estimated absolute pointwise error of $H_{\alpha n}(r)$, $\alpha = \rho, \theta, z$, divided with the largest value of $(|H_{\rho n}(r)|^2 + |H_{\theta n}(r)|^2 + |H_{zn}(r)|^2)^{\frac{1}{2}}$, $r \in A$. The estimated absolute error in $H_{\alpha n}(r)$ is, in turn, taken as the difference between $H_{\alpha n}(r)$ and a reference solution obtained with a mesh containing 50 per cent more quadrature panels and a larger N. Figure 2 also shows that the average

pointwise precision in A has converged to ten digits already at about ten points per wavelength along γ and that it saturates at between 13 and 14 digits. This, rather high, achievable accuracy is only one digit worse than what is reported for the similar, but simpler, acoustic problem in [19] at $k \approx 19$.

Figure 3 shows $H_{\alpha 1}(r)e^{\mathrm{i}\theta}$, $\alpha = \rho, \theta, z$, and $\theta = 0, \pi$, at 490000 field points on a Cartesian grid in the square $x = [-1.2, 1.2]$ and $z = [-1.1, 1.3]$ along with estimated pointwise errors. The experiment uses $n_{\mathrm{pan}} = 71$ in order to assure that the convergence has saturated. The reference solution outside the cavity is the null field $H_{\alpha 1}(r) = 0$, compare (13). The complicated standing wave patterns in the xz-plane, visible in the left images, are typical for eigenfields with large k in combination with small n. Electric and magnetic eigenfields with $n = 0$ and $n = 1$ are non-zero on the symmetry axis in axially symmetric cavities. Since the beam of particles in accelerators travels along the symmetry axis, it interacts strongly with these fields. Eigenfields with $n > 1$ are zero on the symmetry axis and are less important in accelerator technology. It is interesting to observe that the field errors in Figure 3, right images, are comparable to those reported by Barnett [6] for planar Dirichlet Helmholtz problems exterior to objects with diameters ranging from 12 to 100 wavelengths.

The second example concerns and eigenfield with $k = 81.1193972232184$ and $n = 92$. This happens to be the eigenfield with the largest n for $k < 82$. The eigenfields with the largest n for a given k are confined to the parts of the cavity that are farthest from the symmetry axis, as seen in Figure 4. Such fields are called whispering-gallery modes (WGM). They are of very little interest for particle accelerators but have recently become important in nano-optics. See [27] for interesting applications of WGM. Figure 4 depicts the magnetic eigenfields and the corresponding errors. The convergence with mesh refinement (not shown) is similar to that of Figure 2. This is in accordance with our experience that the convergence speed and achievable accuracy of our solver are, more or less, insensitive to n. The WGM are interesting objects to analyze numerically.

6 Conclusion and outlook

We have presented a competitive numerical solver for the determination of normalized magnetic eigenfields in axially symmetric microwave cavities with smooth surfaces. It is based on the following key elements: the magnetic field integral equation, a surface integral for normalization, a Fredholm second kind integral equation for the surface charge density, and a high-order convergent Fourier–Nyström discretization scheme. In the near future, we will extend the solver so that it can determine electric eigenfields. We may also explore the whispering gallery modes of structures that better resemble

those used in nano-optics.

A more challenging task, that we plan to take on, is to extend our solver so that it can handle non-smooth surfaces. Starting in 2008, our group has developed an extremely robust technique for the accurate solution of integral equations on piecewise smooth surfaces – most recently applied to planar scattering problems [18] and to electrostatic problems in $\mathbb{R}^3$ [20]. If applied to the time harmonic Maxwell equations, this technique will enable the accurate determination of eigenfields, and by that the prediction of wakefields, in most types of cavities and flanges used in particle accelerators.

Acknowledgement

This work was supported by the Swedish Research Council under contract 621-2011-5516.

A The normalization integral as a surface integral

It is convenient, and sometimes necessary, to normalize magnetic eigenfields

$$\boldsymbol{H}(\boldsymbol{r}) = \frac{\boldsymbol{H}_n(r)}{\sqrt{2\pi}} e^{\mathrm{i}n\theta} \tag{61}$$

according to (11), that is, such that $\|\boldsymbol{H}\| = 1$. In (61) we have introduced

$$\boldsymbol{H}_n(r) = \boldsymbol{\rho} H_{\rho n}(r) + \boldsymbol{\theta} H_{\theta n}(r) + \boldsymbol{z} H_{zn}(r)\,. \tag{62}$$

Normalized eigenfields are important in wakefield calculations where an eigenfield amplitude is determined by integration along the symmetry axis of the product of the electric eigenfield with a beam current. The normalization integral in (11) is also needed for the extraction of Q-values.

This appendix presents an expression for the normalization integral that is cheaper to evaluate than the volume integral in (11). In fact, the normalization integral will be expressed as a line integral over γ involving readily accessible azimuthal Fourier coefficients. To make (11) hold within our numerical scheme, the coefficients $J_{\tau n}(r)$ and $J_{\theta n}(r)$ obtained from (36) are normalized with the value of $\|\boldsymbol{H}\|$ according to the formulas below. Then the modal representation (37) is automatically consistent with (11).

The scaled electric scalar potential $\Psi(\boldsymbol{r})$ of (55) and the magnetic vector potential $\boldsymbol{\Lambda}(\boldsymbol{r})$ of (56) are related by the Lorenz gauge condition

$$\mathrm{i}k\Psi = \nabla \cdot \boldsymbol{\Lambda}\,. \tag{63}$$

In $\mathbb{R}^3$ the potentials satisfy

$$\nabla^2 \Psi = -k^2 \Psi\,, \tag{64}$$

$$\nabla^2 \boldsymbol{\Lambda} = -k^2 \boldsymbol{\Lambda}\,, \tag{65}$$

$$\boldsymbol{H} = \nabla \times \boldsymbol{\Lambda}\,, \tag{66}$$

and it is easy to show

$$|\nabla \times \boldsymbol{\Lambda}|^2 = \nabla \cdot (\boldsymbol{\Lambda}^* \times (\nabla \times \boldsymbol{\Lambda})) + \mathrm{i}k\nabla \cdot (\boldsymbol{\Lambda}^* \Psi) - k^2|\Psi|^2 + k^2|\boldsymbol{\Lambda}|^2 \,. \quad (67)$$

Let $g(\boldsymbol{r})$ be a Laplace eigenfunction such that $\nabla^2 g = -k^2 g$. Then

$$\begin{aligned} \nabla \cdot (\boldsymbol{r}|g|^2) &= 3|g|^2 + 2\Re\mathrm{e}\{g^*(\boldsymbol{r} \cdot \nabla)g\} \,, \\ \nabla \cdot (\boldsymbol{r}|\nabla g|^2) &= 3|\nabla g|^2 + 2\Re\mathrm{e}\{(\nabla g^* \cdot \nabla)\nabla g \cdot \boldsymbol{r}\} \,, \\ \Re\mathrm{e}\{\nabla \cdot ((\boldsymbol{r} \cdot \nabla)g^* \nabla g)\} &= |\nabla g|^2 - k^2 \Re\mathrm{e}\{g^*(\boldsymbol{r} \cdot \nabla)g\} + \Re\mathrm{e}\{(\nabla g^* \cdot \nabla)\nabla g \cdot \boldsymbol{r}\} \,, \end{aligned}$$

and, by that,

$$|g|^2 = \frac{1}{2k^2} \nabla \cdot \left(\boldsymbol{r} \left(k^2|g|^2 - |\nabla g|^2 \right) + \Re\mathrm{e}\{\nabla g^* (2(\boldsymbol{r} \cdot \nabla) + 1)g\} \right) \,. \quad (68)$$

Now, from (10), (66), (67) and Gauss' theorem one obtains

$$\|\boldsymbol{H}\|^2 = k^2 \left(\|\boldsymbol{\Lambda}\|^2 - \|\Psi\|^2 \right) + \int_\Gamma \boldsymbol{\Lambda}^* \cdot (\boldsymbol{J}_\mathrm{s} + \mathrm{i}k\boldsymbol{\nu}\Psi) \, \mathrm{d}\Gamma \,. \quad (69)$$

The relation (68) with $g(\boldsymbol{r})$ first equal to $\Psi(\boldsymbol{r})$ and then to each of the Cartesian components of $\boldsymbol{\Lambda}(\boldsymbol{r})$, together with (10) and Gauss' theorem, convert the squared norms on the right hand side of (69) to the surface integrals

$$\|\Psi\|^2 = \frac{1}{2k^2} \int_\Gamma \boldsymbol{\nu} \cdot \left(\boldsymbol{r} \left(k^2|\Psi|^2 - |\nabla\Psi|^2 \right) + \Re\mathrm{e}\{\nabla\Psi^* (2(\boldsymbol{r} \cdot \nabla) + 1)\Psi\} \right) \mathrm{d}\Gamma \,, \quad (70)$$

$$\|\boldsymbol{\Lambda}\|^2 = \frac{1}{2k^2} \int_\Gamma \boldsymbol{\nu} \cdot \left(\boldsymbol{r} \left(k^2|\boldsymbol{\Lambda}|^2 - |\nabla\boldsymbol{\Lambda}|^2 \right) + \Re\mathrm{e}\{\nabla\boldsymbol{\Lambda}^* \cdot (2(\boldsymbol{r} \cdot \nabla) + 1)\boldsymbol{\Lambda}\} \right) \mathrm{d}\Gamma \,, \quad (71)$$

where interior limits are to be taken for integrands that are discontinuous at Γ. By this, $\|\boldsymbol{H}\|^2$ is expressed as a surface integral over Γ. We remark that (70) is Barnett's relation [5, equation (12)] generalized to complex-valued eigenfunctions. See also [4, Lemma 3.1], for an $\mathbb{R}^2$ version of (70).

Equation (69) with (10) and (61) can be written in terms of

$$\boldsymbol{\Lambda}_n(r) = \boldsymbol{\rho}\Lambda_{\rho n}(r) + \boldsymbol{\theta}\Lambda_{\theta n}(r) + \boldsymbol{z}\Lambda_{zn}(r) \,, \qquad r \in A \cup \gamma \,, \quad (72)$$

$$\boldsymbol{\Lambda}_n(r) = \boldsymbol{\tau}\Lambda_{\tau n}(r) + \boldsymbol{\theta}\Lambda_{\theta n}(r) + \boldsymbol{\nu}\Lambda_{\nu n}(r) \,, \qquad r \in \gamma \,, \quad (73)$$

$$\boldsymbol{J}_{\mathrm{s}n}(r) = \boldsymbol{\tau}J_{\tau n}(r) + \boldsymbol{\theta}J_{\theta n}(r) \,, \qquad r \in \gamma \,, \quad (74)$$

and $\Psi_n(r)$, $r \in A \cup \gamma$, as

$$\|\boldsymbol{H}\|^2 = k^2 \int_A \left(|\boldsymbol{\Lambda}_n|^2 - |\Psi_n|^2 \right) \rho \, \mathrm{d}A + \int_\gamma \left(\boldsymbol{\Lambda}_n^* \cdot \boldsymbol{J}_{\mathrm{s}n} + \mathrm{i}k\Lambda_{\nu n}^* \Psi_n \right) \rho \, \mathrm{d}\gamma \,. \quad (75)$$

Integration over θ, with $\nabla = \boldsymbol{\tau}(\boldsymbol{\tau}\cdot\nabla) + \boldsymbol{\theta}(\boldsymbol{\theta}\cdot\nabla) + \boldsymbol{\nu}(\boldsymbol{\nu}\cdot\nabla)$, in (70) and (71) gives

$$\begin{aligned}\int_A |\Psi_n|^2\rho\,\mathrm{d}A &= -\frac{1}{2k^2}\int_\gamma \frac{\nu\cdot r}{\rho^2}\left(n^2-k^2\rho^2\right)|\Psi_n|^2\rho\,\mathrm{d}\gamma \\ &\quad -\frac{1}{2k^2}\int_\gamma \nu\cdot r\left(|(\partial_{\boldsymbol{\tau}}\Psi)_n|^2 - |(\partial_{\boldsymbol{\nu}^+}\Psi)_n|^2\right)\rho\,\mathrm{d}\gamma \\ &\quad +\frac{1}{2k^2}\int_\gamma \Re\mathrm{e}\left\{(2\tau\cdot r(\partial_{\boldsymbol{\tau}}\Psi^*)_n + \Psi_n^*)\,(\partial_{\boldsymbol{\nu}^+}\Psi)_n\right\}\rho\,\mathrm{d}\gamma\,, \qquad (76)\\ \int_A |\boldsymbol{\Lambda}_n|^2\rho\,\mathrm{d}A &= -\frac{1}{2k^2}\int_\gamma \frac{\nu\cdot r}{\rho^2}\left((n^2-k^2\rho^2+1)|\boldsymbol{\Lambda}_n|^2 - |\Lambda_{zn}|^2\right)\rho\,\mathrm{d}\gamma \\ &\quad -\frac{1}{2k^2}\int_\gamma \nu\cdot r\left(|(\partial_{\boldsymbol{\tau}}\boldsymbol{\Lambda})_n|^2 - |(\partial_{\boldsymbol{\nu}^+}\boldsymbol{\Lambda})_n|^2 - \frac{4n}{\rho^2}\Im\mathrm{m}\left\{\Lambda_{\rho n}^*\Lambda_{\theta n}\right\}\right)\rho\,\mathrm{d}\gamma \\ &\quad +\frac{1}{2k^2}\int_\gamma \Re\mathrm{e}\left\{(2\tau\cdot r(\partial_{\boldsymbol{\tau}}\boldsymbol{\Lambda}^*)_n + \boldsymbol{\Lambda}_n^*)\cdot(\partial_{\boldsymbol{\nu}^+}\boldsymbol{\Lambda})_n\right\}\rho\,\mathrm{d}\gamma\,, \qquad (77)\end{aligned}$$

where, for directional derivatives of a function $g(\boldsymbol{r})$, we have used

$$\partial_{\boldsymbol{\tau}} g(\boldsymbol{r}) = \boldsymbol{\tau}\cdot\nabla g(\boldsymbol{r})\,, \qquad \boldsymbol{r}\in\Gamma\,, \qquad (78)$$

$$\partial_{\boldsymbol{\nu}^+} g(\boldsymbol{r}^\circ) = \lim_{V\ni\boldsymbol{r}\to\boldsymbol{r}^\circ} \boldsymbol{\nu}^\circ\cdot\nabla g(\boldsymbol{r})\,, \qquad \boldsymbol{r}^\circ\in\Gamma\,. \qquad (79)$$

By this, $\|\boldsymbol{H}\|^2$ is expressed as a line integral over γ. It remains to relate all terms in the integrands of (75), with (76) and (77), to $J_{\tau n}(r)$ and $J_{\theta n}(r)$. This is the topic of Appendix B.

B Ψ and $\boldsymbol{\Lambda}$ and their $\boldsymbol{\tau}$- and $\boldsymbol{\nu}^+$-derivatives

In order to evaluate (75) from the solution to (36), the Fourier coefficients of $\Psi(\boldsymbol{r})$ and $\boldsymbol{\Lambda}(\boldsymbol{r})$, and their derivatives with respect to $\boldsymbol{\tau}$ and $\boldsymbol{\nu}^+$ need to be related to $J_{\tau n}(r)$ and $J_{\theta n}(r)$. This process, which is carried out for $\boldsymbol{H}(\boldsymbol{r})$ in Section 2.4 and Section 3, consists of three steps: First integral representations in terms of $\boldsymbol{J}_{\mathrm{s}}(\boldsymbol{r})$ are found for $\Psi(\boldsymbol{r})$, $\boldsymbol{\Lambda}(\boldsymbol{r})$, and their derivatives; then these representations are expanded in Fourier series; and finally closed-form expressions are constructed for transformed static kernels. This appendix provides additional details on how to obtain the coefficients in (75) and gives complete information for some of them. We also review relations that offer simpler and more accurate coefficient evaluation in certain situations.

The integral representation of $\boldsymbol{\Lambda}(\boldsymbol{r})$ in terms of $\boldsymbol{J}_{\mathrm{s}}(\boldsymbol{r})$ is given by (56). For $\boldsymbol{r}\in\Gamma$, the derivatives of $\boldsymbol{\Lambda}(\boldsymbol{r})$ with respect to $\boldsymbol{\tau}$ and $\boldsymbol{\nu}^+$ are

$$\partial_{\boldsymbol{\tau}}\boldsymbol{\Lambda}(\boldsymbol{r}) = K_{\boldsymbol{\tau}}\boldsymbol{J}_{\mathrm{s}}(\boldsymbol{r})\,, \qquad \boldsymbol{r}\in\Gamma\,, \qquad (80)$$

$$\partial_{\boldsymbol{\nu}^+}\boldsymbol{\Lambda}(\boldsymbol{r}) = \frac{1}{2}\boldsymbol{J}_{\mathrm{s}}(\boldsymbol{r}) + K_{\boldsymbol{\nu}}\boldsymbol{J}_{\mathrm{s}}(\boldsymbol{r})\,, \qquad \boldsymbol{r}\in\Gamma\,, \qquad (81)$$

where the operators

$$K_{\boldsymbol{\tau}} g(\boldsymbol{r}) = \int_\Gamma \boldsymbol{\tau} \cdot \nabla \Phi_k(\boldsymbol{r}, \boldsymbol{r}') g(\boldsymbol{r}') \, \mathrm{d}\Gamma' \,, \tag{82}$$

$$K_{\boldsymbol{\nu}} g(\boldsymbol{r}) = \int_\Gamma \boldsymbol{\nu} \cdot \nabla \Phi_k(\boldsymbol{r}, \boldsymbol{r}') g(\boldsymbol{r}') \, \mathrm{d}\Gamma' \,, \tag{83}$$

introduced in [19], are of the double-layer type (19). In particular,

$$D_{\boldsymbol{\nu}}(\boldsymbol{r}, \boldsymbol{r}') = -\frac{(\nu \cdot (r - r') + \nu_\rho \rho' \, (1 - \cos(\theta - \theta')))}{4\pi |\boldsymbol{r} - \boldsymbol{r}'|^3} \,, \tag{84}$$

$$D_{\boldsymbol{\nu} n}(r, r') = \eta \left[d(\nu) \mathfrak{R}_n(\chi) - \frac{\nu_\rho}{2\rho} \left(\mathfrak{R}_n(\chi) + \mathfrak{Q}_{n-\frac{1}{2}}(\chi) \right) \right] . \tag{85}$$

The integral representation of $\Psi(\boldsymbol{r})$ in terms of $\boldsymbol{J}_{\mathrm{s}}(\boldsymbol{r})$ is given by (55) with (57). In order to avoid the numerical differentiation associated with (57) we follow [29] and derive a Fredholm second kind integral equation for $\varrho_{\mathrm{s}}(\boldsymbol{r})$ based on the observation that

$$\lim_{V \ni \boldsymbol{r} \to \boldsymbol{r}^\circ} \boldsymbol{\nu}^\circ \cdot \boldsymbol{E}(\boldsymbol{r}) = -\varrho_{\mathrm{s}}(\boldsymbol{r}^\circ) \,, \qquad \boldsymbol{r}^\circ \in \Gamma \,, \tag{86}$$

$$\boldsymbol{E}(\boldsymbol{r}) = \mathrm{i}k \boldsymbol{\Lambda}(\boldsymbol{r}) - \nabla \Psi(\boldsymbol{r}) \,, \qquad \boldsymbol{r} \in \mathbb{R}^3 \setminus \Gamma \,, \tag{87}$$

where $\boldsymbol{E}(\boldsymbol{r})$ is the electric field divided by the free space wave impedance. From (55), (83), and (87) we get

$$\lim_{V \ni \boldsymbol{r} \to \boldsymbol{r}^\circ} \boldsymbol{\nu}^\circ \cdot \boldsymbol{E}(\boldsymbol{r}) = \mathrm{i}k \boldsymbol{\Lambda}_{\boldsymbol{\nu}}(\boldsymbol{r}^\circ) - \frac{1}{2} \varrho_{\mathrm{s}}(\boldsymbol{r}^\circ) - K_{\boldsymbol{\nu}} \varrho_{\mathrm{s}}(\boldsymbol{r}^\circ) \,, \qquad \boldsymbol{r}^\circ \in \Gamma \,, \tag{88}$$

and combine this with (86) to obtain an integral equation which in modal form reads

$$\left(I - 2\sqrt{2\pi} K_{\boldsymbol{\nu} n} \right) \varrho_{sn}(r) = -2\mathrm{i}k \Lambda_{\nu n}(r) \,, \qquad r \in \gamma \,. \tag{89}$$

From (9), expressed in terms of $\boldsymbol{E}(\boldsymbol{r})$ as

$$\lim_{V \ni \boldsymbol{r} \to \boldsymbol{r}^\circ} \boldsymbol{\nu}^\circ \times \boldsymbol{E}(\boldsymbol{r}) = \boldsymbol{0} \,, \qquad \boldsymbol{r}^\circ \in \Gamma \,, \tag{90}$$

and (87) we obtain

$$\partial_{\boldsymbol{\tau}} \Psi(\boldsymbol{r}) = \mathrm{i}k \Lambda_\tau(\boldsymbol{r}) \,, \qquad \boldsymbol{r} \in \Gamma \,, \tag{91}$$

$$\partial_{\boldsymbol{\theta}} \Psi(\boldsymbol{r}) = \mathrm{i}k\rho \Lambda_\theta(\boldsymbol{r}) \,, \qquad \boldsymbol{r} \in \Gamma \,. \tag{92}$$

The Fourier coefficients of these relations read

$$(\partial_{\boldsymbol{\tau}} \Psi)_n(r) = \mathrm{i}k \Lambda_{\tau n}(r) \,, \qquad r \in \gamma \,, \tag{93}$$

$$n \Psi_n(r) = \rho k \Lambda_{\theta n}(r) \,, \qquad r \in \gamma \,, \tag{94}$$

and are used for the evaluation of $(\partial_{\boldsymbol{\tau}}\Psi)_n(r)$ and of $\Psi_n(r)$, $n \neq 0$.

Explicit expressions in terms of $J_{\tau n}(r)$ and $J_{\theta n}(r)$ for the coefficients of $\boldsymbol{\Lambda}(\boldsymbol{r})$, with basis as in (73), are

$$\Lambda_{\tau n}(r) = \sqrt{2\pi}S_{1n}J_{\tau n}(r) + \mathrm{i}\sqrt{2\pi}S_{2n}J_{\theta n}(r)\,, \tag{95}$$

$$\Lambda_{\theta n}(r) = \mathrm{i}\sqrt{2\pi}S_{3n}J_{\tau n}(r) + \sqrt{2\pi}S_{4n}J_{\theta n}(r)\,, \tag{96}$$

$$\Lambda_{\nu n}(r) = \sqrt{2\pi}S_{5n}J_{\tau n}(r) + \mathrm{i}\sqrt{2\pi}S_{6n}J_{\theta n}(r)\,, \tag{97}$$

where

$$S_{\alpha n}g_n(r) = \int_\gamma S_{\alpha n}(r,r')g_n(r')\rho'\,\mathrm{d}\gamma'\,, \qquad \alpha = 1,\ldots,6\,, \tag{98}$$

and $S_{\alpha n}(r,r')$ are transformed kernels of operators S_α of the form (58). The static kernels $Z_\alpha(\boldsymbol{r},\boldsymbol{r}')$ are

$$Z_1(\boldsymbol{r},\boldsymbol{r}') = \left(\nu_z\nu_z'\cos(\theta-\theta') + \nu_\rho\nu_\rho'\right)\Phi_0(\boldsymbol{r},\boldsymbol{r}')\,, \tag{99}$$

$$Z_2(\boldsymbol{r},\boldsymbol{r}') = -\mathrm{i}\nu_z\sin(\theta-\theta')\Phi_0(\boldsymbol{r},\boldsymbol{r}')\,, \tag{100}$$

$$Z_3(\boldsymbol{r},\boldsymbol{r}') = \mathrm{i}\nu_z'\sin(\theta-\theta')\Phi_0(\boldsymbol{r},\boldsymbol{r}')\,, \tag{101}$$

$$Z_4(\boldsymbol{r},\boldsymbol{r}') = \cos(\theta-\theta')\Phi_0(\boldsymbol{r},\boldsymbol{r}')\,, \tag{102}$$

$$Z_5(\boldsymbol{r},\boldsymbol{r}') = \left(\nu_\rho\nu_z'\cos(\theta-\theta') - \nu_z\nu_\rho'\right)\Phi_0(\boldsymbol{r},\boldsymbol{r}')\,, \tag{103}$$

$$Z_6(\boldsymbol{r},\boldsymbol{r}') = -\mathrm{i}\nu_\rho\sin(\theta-\theta')\Phi_0(\boldsymbol{r},\boldsymbol{r}')\,, \tag{104}$$

with closed-form Fourier coefficients

$$Z_{1n}(r,r') = \eta\left[\frac{\nu_z\nu_z'}{2}\left(\mathfrak{Q}_{n-\frac{3}{2}}(\chi) + \mathfrak{Q}_{n+\frac{1}{2}}(\chi)\right) + \nu_\rho\nu_\rho'\mathfrak{Q}_{n-\frac{1}{2}}(\chi)\right]\,, \tag{105}$$

$$Z_{2n}(r,r') = -\eta\frac{\nu_z}{2}\left(\mathfrak{Q}_{n-\frac{3}{2}}(\chi) - \mathfrak{Q}_{n+\frac{1}{2}}(\chi)\right)\,, \tag{106}$$

$$Z_{3n}(r,r') = \eta\frac{\nu_z'}{2}\left(\mathfrak{Q}_{n-\frac{3}{2}}(\chi) - \mathfrak{Q}_{n+\frac{1}{2}}(\chi)\right)\,, \tag{107}$$

$$Z_{4n}(r,r') = \eta\frac{1}{2}\left(\mathfrak{Q}_{n-\frac{3}{2}}(\chi) + \mathfrak{Q}_{n+\frac{1}{2}}(\chi)\right)\,, \tag{108}$$

$$Z_{5n}(r,r') = \eta\left[\frac{\nu_\rho\nu_z'}{2}\left(\mathfrak{Q}_{n-\frac{3}{2}}(\chi) + \mathfrak{Q}_{n+\frac{1}{2}}(\chi)\right) - \nu_z\nu_\rho'\mathfrak{Q}_{n-\frac{1}{2}}(\chi)\right]\,, \tag{109}$$

$$Z_{6n}(r,r') = -\eta\frac{\nu_\rho}{2}\left(\mathfrak{Q}_{n-\frac{3}{2}}(\chi) - \mathfrak{Q}_{n+\frac{1}{2}}(\chi)\right)\,. \tag{110}$$

For $\Psi_0(r)$ and for $(\partial_{\boldsymbol{\nu}^+}\Psi)_n(r)$ we use

$$\Psi_0(r) = \sqrt{2\pi}S_{\varsigma 0}\varrho_{\mathrm{s}0}(r)\,, \qquad r\in\gamma\,, \tag{111}$$

$$(\partial_{\boldsymbol{\nu}^+}\Psi)_n(r) = \varrho_{\mathrm{s}n}(r) + \mathrm{i}k\Lambda_{\nu n}(r)\,, \qquad r\in\gamma\,, \tag{112}$$

with $\varrho_{\mathrm{s}n}(r)$ from (89).

C Code for toroidal harmonics

The MATLAB function `toroharm` is a modification of the standard MATLAB function `ellipke`. It returns accurate values of $\mathfrak{Q}_{n-\frac{1}{2}}(\chi)$ for $n = 0, 1$

```
function [QA,QB]=toroharm(chi,b0)
a0 = 1;
s0 = 0;
i1 = 0.5;
w1 = 1;
while max(w1(:)) > eps
  w1 = i1*(a0-b0).^2;
  s0 = s0+w1;
  a1 = a0+b0;
  b0 = sqrt(a0.*b0);
  a0 = a1/2;
  i1 = 2*i1;
end
mu = sqrt(2./(chi+1));
QA = pi*mu./a1;
QB = pi*s0./(mu.*a1);
```

The output arguments `QA` and `QB` correspond to $\mathfrak{Q}_{-\frac{1}{2}}(\chi)$ and $\mathfrak{Q}_{\frac{1}{2}}(\chi)$. The input argument `chi` corresponds to χ and the input argument `b0` should be chosen as

$$\texttt{b0} = \sqrt{\frac{\chi - 1}{\chi + 1}}\,. \tag{113}$$

The reason for providing `b0` as an extra input argument is that this quantity may be available to higher relative precision than what comes from a direct evaluation via χ and (113). Compare (41) when $|r - r'|$ is small.

References

[1] A. Abdelmageed, 'Efficient evaluation of modal Green's functions arising in EM scattering by bodies of revolution', Prog. Electromagn. Res., **27**, 337–356 (2000)

[2] M. G. Andreasen, 'Scattering from bodies of revolution', IEEE Trans. Antennas Propag., **13**, 303–310 (1965)

[3] R. Ballantini, et al., 'A detector of high frequency gravitational waves based on coupled microwave cavities', Class. Quantum Grav., **20**, 3505–3522 (2003)

[4] A. H. Barnett, 'Asymptotic rate of quantum ergodicity in chaotic Euclidean billiards', Commun. Pur. Appl. Math., **59**, 1457–1488 (2006)

[5] A. H. Barnett, 'Quasi-orthogonality on the boundary for Euclidean Laplace eigenfunctions', arXiv:math-ph/0601006 (2006)

[6] A. H. Barnett, 'Evaluation of layer potentials close to the boundary for Laplace and Helmholtz problems on analytic planar domains', SIAM J. Sci. Comput., **36**, A427–A451 (2014)

[7] W. Bartky, 'Numerical calculation of a generalized complete elliptic integral', Rev. Mod. Phys., **10**, 264–269 (1938)

[8] W. Bruns, 'GdfidL: A finite difference program with reduced memory and CPU usage', Proceedings 1997 Particle Accelerator Conference, Vol. 2, 2651–2653 (1998)

[9] H. S. Cohl and J. E. Tohline, 'A compact cylindrical Green's function expansion for the solution of potential problems', Astrophys. J., **527**, 86–101 (1999)

[10] C. Epstein, and L. Greengard, 'Debye sources and the numerical solution of the time harmonic Maxwell equations', Commun. Pur. Appl. Math., **63**, 413–463 (2010)

[11] C. Epstein, L. Greengard, and M. O'Neil 'Debye sources and the numerical solution of the time harmonic Maxwell equations II', Commun. Pur. Appl. Math., **66**, 753–789 (2013)

[12] J. L. Fleming, A. W. Wood, and W. D. Wood Jr, 'Locally corrected Nyström method for EM scattering by bodies of revolution', J. Comput. Phys., **196**, 41–52 (2004)

[13] D. J. Gargas, et al., 'Whispering gallery mode lasing from zinc oxide hexagonal nanodisks', ACS Nano, **4**, 3270-3276 (2010)

[14] S. D. Gedney, and R. Mittra, 'The use of the FFT for the efficient solution of the problem of electromagnetic scattering by a body of revolution', IEEE Trans. Antennas Propag., **38**, 313–322 (1990)

[15] A. W. Glisson and D. R. Wilton, 'Simple and efficient numerical techniques for treating bodies of revolution', Mississippi Univ. RADC-TR-79-22, (1979)

[16] K. Halbach and R. F. Holsinger, 'SUPERFISH – a computer program for evaluation of RF cavities with cylindrical symmetry', Part. Accel., **7**, 213–222 (1976)

[17] J. Helsing and A. Holst, 'Variants of an explicit kernel-split panel-based Nyström discretization scheme for Helmholtz boundary value problems', arXiv:1311.6258v2 [math.NA] (2014)

[18] J. Helsing and A. Karlsson, 'An accurate boundary value problem solver applied to scattering from cylinders with corners', IEEE Trans. Antennas Propag., **61**, 3693–3700 (2013)

[19] J. Helsing and A. Karlsson, 'An explicit kernel-split panel-based Nyström scheme for integral equations on axially symmetric surfaces', J. Comput. Phys., **272**, 686-703 (2014)

[20] J. Helsing and K-. M. Perfekt, 'On the polarizability and capacitance of the cube', Appl. Comput. Harmon. Anal., **34**, 445–468 (2013)

[21] A. A. Kucharski, 'A method of moments solution for electromagnetic scattering by inhomogeneous dielectric bodies of revolution', IEEE Trans. Antennas Propag., **48**, 1202–1210 (2000)

[22] J. R. Mautz and R. F. Harrington, 'Radiation and scattering from bodies of revolution', Appl. Sci. Res., **20**, 405–435 (1969)

[23] P. Ylä-Oijala, 'Comparison of boundary integral formulations for field computation in axisymmetric resonators', J. Electromagnet. Wave., **14**, 767–793 (2000)

[24] J. Segura and A. Gil, 'Evaluation of toroidal harmonics', Comput. Phys. Commun., **124**, 104–122 (2000)

[25] J. A. Stratton, Electromagnetic Theory, McGraw-Hill, New York, 1941

[26] J. A. Stratton and L. J. Chu, 'Diffraction theory of electromagnetic waves', Phys. Rev., **56**, 99–107 (1939)

[27] A. C. Tamboli, et al., 'Room-temperature continuous-wave lasing in GaN/InGaN microdisks', Nature Photon., **1**, 61–64 (2006)

[28] M. S. Tong and W. C. Chew, 'Evaluation of singular Fourier coefficients in solving electromagnetic scattering by body of revolution', Radio Sci., **43**, RS4003 (2008)

[29] F. Vico, Z. Gimbutas, L. Greengard, and M. Ferrando-Bataller, 'Overcoming low-frequency breakdown of the magnetic field integral equation', IEEE Trans. Antennas Propag., **61**, 1285–1290 (2013)

[30] T. P. Wangler, 'RF Linear accelerators', 2nd ed., Wiley-VCH, Weinheim, 2008

[31] P. C. Waterman, 'Symmetry, Unitarity, and Geometry in Electromagnetic Scattering', Phys. Rev. D, **4**, 825–839 (1971)

[32] G. Wen, 'Time-domain theory of metal cavity resonator', Prog. Electromagn. Res., **78**, 219–253 (2008)

[33] T. Weiland, 'A discretization method for the solution of Maxwell's equations for six-component Fields', AEU-Int. J. Electron. C., **31**, 116–120 (1977)

[34] P. Young, S. Hao, and P.G. Martinsson, 'A high-order Nyström discretization scheme for boundary integral equations defined on rotationally symmetric surfaces', J. Comput. Phys., **231**, 4142–4159 (2012)